Proceedings of the 28th IEEE
EMBS Annual International Conference
New York City, USA, Aug 30-Sept 3, 2006

Autofocusing for Automated Microscopic Evaluation of Blood Smear and Pap Smear

X.Y. Liu, *Student Member, IEEE*, W.H. Wang, and Y. Sun, *Member, IEEE*

Abstract – **Autofocusing is a fundamental procedure towards automated microscopic evaluation of blood smear and pap smear samples for clinical diagnosis. This paper presents comparison results of 16 focus algorithms based on a total of 8000 bright-field images from 10 blood smear and pap smear samples. A ranking methodology adapted from our previously proposed ranking system is used for thoroughly evaluating the performance of the selected 16 focus algorithms. Experimental results demonstrate that the Variance algorithm provides the best overall performance, which will be selected for our future implementation of an automated microscopic system for computer-assisted blood smear and pap smear evaluation. Together with our previously reported findings, we hypothesize that the Variance algorithm or the Normalized Variance algorithm is the optimal focus algorithm for all non-fluorescence microscopy applications.**

I. Introduction

MANUAL microscopic examination of hundreds or thousands of blood smear and pap smear samples is routinely performed by cytotechnologists and pathologists in clinical and hospital laboratory environments. Pap smear that is a sample with cervical cells on a glass slide, is the most important diagnostic technique for detecting pre-invasive cervical cancer. Peripheral blood smear provides information on the number and shape of blood cells for detecting blood-related diseases such as anemia and leukemia.

Advances have been made to make smear interpretation more descriptive, paving the foundation to the realization of fully automated computer-assisted microscopic diagnosis [1] [2]. Fully automated microscopic diagnosis is attractive as it will not only alleviate the tremendous workload from medical professionals (e.g., each pap smear contains roughly 50,000 to 300,000 cells) and results in greater efficiency; but more importantly, an autotomated microscopic diagnostic system will be capable of encompassing expert knowledge from diverse specialties within pathology to detect a multitude of diseases or a comprehensive disease pattern. Towards the realization of fully automated microscopic diagnosis, autofocusing is a fundamental procedure to perform.

Although autofocusing is a long standing research topic and many focus algorithms have been proposed, the selection of the optimal algorithm for specific experimental microscopy applications remains *ad hoc*. The AutoCorrelation algorithm was found to be the optimal focus algorithm for fluorescence microscopy applications [3][4]. We previously demonstrated that the Normalized Variance algorithm provided the best performance for several types of non-fluorescence samples [5].

The authors are with the Advanced Micro and Nanosystems Laboratory at the University of Toronto. 5 King's College Road, Toronto, Ontario, Canada, M5S 3G8 (phone: 1-416-946-0549; e-mail: sun@mie.utoronto.ca)

As the selection of the optimal autofocusing algorithm appears to be application specific, this paper focuses on the determination of the optimal focus algorithm for pap smear and blood smear bright-field imaging through a systematic evaluation of 16 commonly used focus algorithms that are applied to a total of 8000 bright-field microscopic images.

II. Materials and Method

Ten samples (five blood smears; five pap smears) shown in Fig. 1 were employed for testing. These representative samples include a variety of information, from which a general conclusion can be drawn. The five blood smear samples were prepared in the Princess Margaret Hospital (Toronto, Canada), and the five pap smear samples were prepared in the Sunnybrook Health Sciences Centre and Women's College Hospital (Toronto, Canada). The thickness is 10~15μm for the blood smear samples and 15~20μm for the pap smear samples.

The experimental setup consists of a motorized inverted microscope (Olympus IX81), a CMOS digital camera (Basler A601f), and an image processing computer (3.2GHz CPU with 1.0GB RAM). The minimum focus step of the motorized microscope is 0.01μm. The camera has a pixel size of 9.9×9.9μm. A 40× objective (Olympus LUCPlanFLN, 1.9μm depth of field, NA 0.6, and 0.5μm resolution) and the bright-field observation method were used. The total magnification of the observation system including magnification effects of objective, coupler, and camera is 40×. Multiplying this 40× with the objective's 0.5μm resolution, one can confirm that the pixel size of the camera (9.9μm) satisfies the Nyquist theorem. Thus, there is no frequency aliasing in image acquisition.

Ten image sets corresponding to the ten samples were collected with a step of 0.25μm. Each set contains 800 images (640×480), and a total of 8000 images were processed using the 16 focus algorithms discussed in the following section.

III. Focus Algorithms

A common rationale of focus algorithms is that focused images contain more information and details (e.g., edges) than unfocused images, based on which an objective function indicating the sharpness of images is used to evaluate the degree of focusing. The focus position is obtained when the objective function reaches its extremum. In this study, the most commonly used 16 focus algorithms were compared to determine the optimal focus algorithm for pap smear and blood smear bright-field imaging. These algorithms can be classified into four groups [5]. In order to

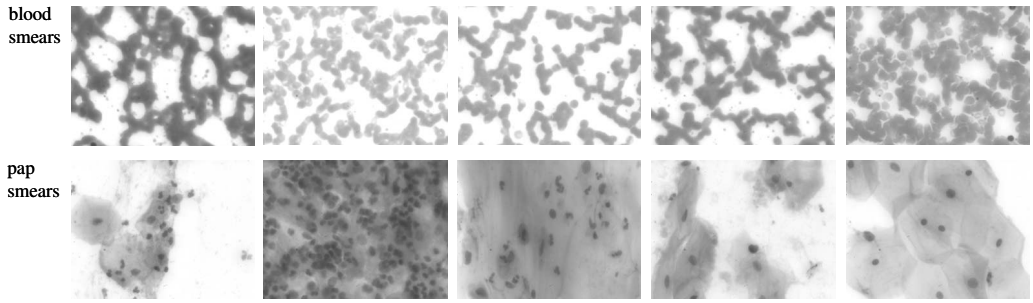

Fig. 1 Bright-field images of 5 blood smear (top) and 5 pap smear (bottom) samples.

make the paper self-contained and facilitate the discussion in Section V, these 16 selected algorithms are briefly summarized as follows.

A. Derivative-based Algorithms

Thresholded absolute gradient [6]: the absolute value of first derivative is accumulated when it is larger than a pre-defined threshold v:

$$F_{thre\_grad} = \sum_{height}\sum_{width} \left| i(x+1, y) - i(x, y) \right| \tag{A-1}$$

where $i(x, y)$ is the gray level intensity of pixel (x, y), and $\left| i(x+1, y) - i(x, y) \right| \geq v$.

Squared Gradient [6]:

$$F_{squa\_grad} = \sum_{height}\sum_{width} \left(i(x+1, y) - i(x, y) \right)^2 \tag{A-2}$$

where $\left(i(x+1, y) - i(x, y) \right)^2 \geq v$.

Brenner gradient [7]:

$$F_{Brenner} = \sum_{height}\sum_{width} \left(i(x+2, y) - i(x, y) \right)^2 \tag{A-3}$$

where $\left(i(x+2, y) - i(x, y) \right)^2 \geq v$.

Tenenbaum gradient [8][9]:

$$F_{Tenengrad} = \sum_{height}\sum_{width} \left(S_x(x, y)^2 + S_y(x, y)^2 \right) \tag{A-4}$$

where $S_x(x, y)$ and $S_y(x, y)$ are the convoluted images with Sobel operators.

Energy Laplace [10]: the second derivative $C(x, y)$ is computed by convolving an image with the convolution mask:

$$L = \begin{bmatrix} -1 & -4 & -1 \\ -4 & 20 & -4 \\ -1 & -4 & -1 \end{bmatrix}$$

and the objective function is

$$F_{energy\_laplace} = \sum_{height}\sum_{width} C(x, y)^2 \tag{A-5}$$

Sum of modified Laplace [11]:

$$F_{SML} = \sum_{height}\sum_{width} \left(\left| L_x(x, y) \right| + \left| L_y(x, y) \right| \right) \tag{A-6}$$

where $L(x, y)$ are convoluted images with Laplacian operators.

Sum of squared Gaussian derivatives [12]:

$$F_{sum\_Gaus\_deri} = \frac{1}{MN} \sum_{height}\sum_{width} \left(G_x(\sigma)^2 + G_y(\sigma)^2 \right) \tag{A-7}$$

where $G_x(\sigma)$ and $G_y(\sigma)$ are first-order Gaussian derivatives in horizontal/vertical directions. The scale can be determined by $\sigma = d / 2\sqrt{3}$, where d is dimension of the smallest feature.

B. Statistical Algorithms

Variance [8][13]:

$$F_{variance} = \frac{1}{H \cdot W} \sum_{height}\sum_{width} \left(i(x, y) - \bar{i} \right)^2 \tag{A-8}$$

where $\bar{i}$ is the mean intensity of the image, and H and W are image height and width.

Normalized variance [8][13]:

$$F_{variance} = \frac{1}{H \cdot W \cdot \bar{i}} \sum_{height}\sum_{width} \left(i(x, y) - \bar{i} \right)^2 \tag{A-9}$$

Autocorrelation [3][4]:

$$F_{auto\_corr} = \sum_{height}\sum_{width} i(x, y) \cdot i(x+1, y) - \sum_{height}\sum_{width} i(x, y) \cdot i(x+2, y) \tag{A-10}$$

Standard deviation-based correlation [3][4]:

$$F_{stddev\_corr} = \sum_{height}\sum_{width} i(x, y) \cdot i(x+1, y) - H \cdot W \cdot \bar{i}^2 \tag{A-11}$$

C. Histogram-based Algorithms

Range algorithm [14]: Denote the number of pixels with intensity i by $h_k(i)$, the objective function is

$$F_{range} = \max\left\{ i \,\middle|\, h(i) > 0 \right\} - \min\left\{ i \,\middle|\, h(i) > 0 \right\} \tag{A-12}$$

Entropy [14]:

$$F_{entropy} = -\sum_{i} p_i \cdot \log_2(p_i) \tag{A-13}$$

where $p_i = h(i) / H \cdot W$.

D. Intuitive Algorithms

Thresholded content [13][15]: objective function of this algorithm is the sum of intensities above a certain threshold.

$$F_{thre\_cont} = \sum_{height}\sum_{width} i(x, y) \tag{A-14}$$

where $i(x, y) \geq v$.

Thresholded pixel count [13]:

$$F_{pixel\_count} = \sum_{height}\sum_{width} c\left(i(x, y), v \right) \tag{A-15}$$

where $c\left(i(x, y), v \right) = \begin{cases} 1, & i(x, y) \leq v \\ 0, & else \end{cases}$.

Image power [6]:

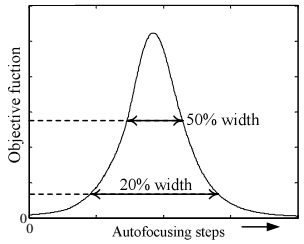

Fig. 2 Objective function curve of the focus algorithms.

$$F_{power} = \sum_{height} \sum_{width} i(x,y)^2 \qquad \text{(A-16)}$$

where $i(x,y) \geq v$.

IV. Ranking Methodology

The following criteria including monotonicity and single modality are used for evaluating the 16 focus algorithms. Each focus algorithm produces a focus curve for an image set. To quantitatively compare these algorithms, all focus curves were normalized, and the curves with global minimum inverted.

A) Accuracy: This criterion is described by the distance between the real focus position, manually determined by a proficient microscopy operator, and the global maximum position of the objective function curve.

B) Number of Local Maxima: The local maxima may trap the autofocusing algorithm, and increase the computational complexity. This criterion represents the number of local maxima in a focus curve. The less this measure is, the easier and faster it is to reach the global maximum.

C) Range: This criterion measures the distance between two neighboring local minima around the global maximum. A larger range measure allows for easier searching of the maximum of the focusing curve.

D) Noise Level: This criterion describes the speed of the direction changes (second derivative of the focusing curve) between local maxima. The sum of squared second derivatives except the value at the maximum is used to quantitatively represent this measure. A focus curve with lower noise level guarantees the accuracy of the adaptively step-size-adjusting algorithm, such as forward Euler integration to determine the next position of the focusing motor in microscope.

E) Width at 50% Max.: This criterion measures the width at 50% maximum of the focus curve. The smaller it is, the shaper the focus peak is, and the easier it is to locate the focus position accurately.

F) Width at 20% Max.: Besides the above 5 criteria that were described previously in [5], the width at 20% maximum (Fig. 2) is also employed in this study to evaluate the performance of focus algorithms, which is of great importance for providing search algorithms with slope clues in a wide range to rapidly locate the global maximum [13].

G) Overall Score: The ideal values for the 6 individual criteria are given in Table I, in which the ideal values for the *range* and the *20% width criteria* are the total number of images in each image set (800 in this study for each image set). To evaluate a focus algorithm, the difference/distance between each criterion's ideal value and the value of the focus curve is calculated. An ideal focus curve has criterion distance coordinates of [0, 0, 0, 0, 0, 0]. The lower a criterion distance, the better the performance of a algorithm under this criterion. In order to maintain equal weights for each criterion distance, all the individual criterion distances are normalized. The overall score is defined as the Euclidean distance of a focus curve to [0, 0, 0, 0, 0, 0].

TABLE I IDEAL VALUES FOR INDIVIDUAL RANKING CRITERIA

Criteria	accuracy	# of local max	Range	noise level	50% width	20% width
Ideal value	0	0	800	0	0	800

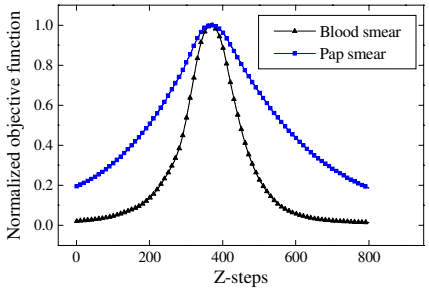

Fig. 3 Focus curves of Variance algorithm for single image sets of blood smear and pap smear

V. Results and Discussion

A total of 8000 images collected from the ten blood smear and pap smear samples (Fig. 1) were processed using the 16 selected algorithms. The selected threshold values for algorithms (A-14), (A-15), (A-16) are 150, 170, and 180, which were selected because the algorithms provide their best performance with these threshold values. It has been demonstrated that algorithms (A-1)~(A-3) do not require thresholding [5]. According to the dimension of the smallest feature, scale σ in algorithm (A-7) was set to be one pixel.

The 16 algorithms were scored and ranked based on their focus curves of blood smear and pap smear according to both individual criteria and overall scores. The ranking results are listed in Table II and III. Every entry in these data tables represents the average value from five focus curves. Lower values in all columns of the tables in this section represent better performance. The numbers in parentheses represent the ranking of a focus algorithm according to individual criterion distances (column #2-#7) or the overall score (column #8).

Based on the ranking results, it can be seen that the Variance algorithm (A-8) provides the best overall performance for both blood and pap smear. Fig. 3 shows the focus curves of the Variance algorithm for one image set of blood and pap smear. The Normalized Variance algorithm (A-9) provides nearly optimal overall performance for both types of samples, which is in agreement with our previous findings for other types of samples [5].

The best overall performance of the algorithms (A-8), (A-9), and (A-11) is mainly due to the fact that these statistical-based algorithms are less noise sensitive. This noise insensitivity property enables these algorithms to produce the lowest number of local maxima, the best range,

TABLE II BLOOD SMEAR: RANKING OF 16 FOCUS ALGORITHMS ACCORDING TO INDIVIDUAL CRITERIA AND OVERALL SCORE

Algorithm	Accuracy	# of local max	Range	Noise level	50% width	20% width	Overall score
ThreAbsGrad (A-1)	4.2(1)	204.0(13)	787(13)	0.00573000(12)	162.6(12)	603.6(11)	1.6136(13)
SquaGrad (A-2)	5.0(4)	204.2(14)	710(9)	0.00734000(13)	75.6(1)	595.2(10)	1.5222(10)
BrennerGrad (A-3)	4.6(3)	168.6(9)	560.6(6)	0.00116000(9)	88.8(3)	646.2(15)	1.3882(7)
TeneGrad (A-4)	4.4(2)	136.0(7)	485.8(5)	0.00051949(8)	92.0(4)	641.2(14)	1.2718(5)
EnergyLapl (A-5)	26.8(7)	239.0(16)	793.8(16)	0.07802000(15)	137.8(7)	464.0(5)	1.6419(15)
SumModiLapl (A-6)	28.6(9)	217.2(15)	793.4(15)	0.02176000(14)	149.4(8)	452.2(3)	1.5666(12)
SumGausDeri (A-7)	5.2(5)	103.4(5)	384.4(3)	0.00023327(6)	97.2(5)	635.4(13)	1.1532(4)
Variance (A-8)	30.0(10)	1.2(1)	315.8(1)	0.00009414(2)	159.2(10)	498.8(7)	0.9481(1)
NormVariance (A-9)	30.6(13)	1.2(1)	315.8(1)	0.00010423(5)	156.8(9)	502.0(9)	0.9522(2)
AutoCorr (A-10)	6.0(6)	146.6(8)	592.2(7)	0.0017000(10)	103.8(6)	611(12)	1.3350(6)
StanDeviCorr (A-11)	30.0(10)	1.2(1)	475.4(4)	0.00009435(3)	159.2(10)	498.8(7)	1.0484(3)
Range (A-12)	47.2(15)	178.8(10)	788.4(14)	0.28680000(16)	407.2(15)	203.6(2)	1.8886(16)
EntrAlgo (A-13)	93.4(16)	12.6(4)	606.6(8)	0.00007616(1)	495.2(16)	114(1)	1.6170(14)
ThreCont (A-14)	40.0(14)	181.2(11)	775(11)	0.00010348(4)	212.6(14)	458.8(4)	1.5322(11)
ThrePixeCont (A-15)	30.2(12)	106.2(6)	725.8(10)	0.00402000(11)	82.2(2)	682.6(16)	1.4717(8)
ImagePower (A-16)	26.8(7)	186.0(12)	777.4(12)	0.00041263(7)	162.6(12)	479.4(6)	1.4994(9)

TABLE III PAP SMEAR: RANKING OF 16 FOCUS ALGORITHMS ACCORDING TO INDIVIDUAL CRITERION AND OVERALL SCORE

Algorithm	Accuracy	# of local max	Range	Noise level	50% width	20% width	Overall score
ThreAbsGrad (A-1)	5.0(5)	241.6(14)	778.4(10)	0.010650(11)	223.4(8)	513.6(11)	1.6410(13)
SquaGrad (A-2)	4.4(4)	236.6(13)	762.4(9)	0.019500(14)	61.4(1)	340.6(10)	1.4202(6)
BrennerGrad (A-3)	3.8(2)	201.6(11)	701.6(6)	0.006240(5)	71.2(2)	659.0(15)	1.5316(10)
TeneGrad (A-4)	3.8(2)	182.4(10)	619.6(2)	0.003100(9)	75.2(3)	653.8(14)	1.4336(7)
EnergyLapl (A-5)	100.6(14)	262.2(15)	793.4(14)	0.050070(15)	367.4(13)	211.2(3)	1.9931(16)
SumModiLapl (A-6)	102.0(15)	262.8(16)	793.6(15)	0.017150(12)	346.4(12)	144.8(1)	1.9549(15)
SumGausDeri (A-7)	3.6(1)	148.0(6)	556.4(1)	0.001040(7)	82.6(4)	642.2(13)	1.3218(4)
Variance (A-8)	29.8(8)	5.2(3)	668.8(3)	0.000125(2)	252.6(9)	280.4(8)	1.1678(1)
NormVariance (A-9)	29.8(8)	4.8(1)	718.4(7)	0.000122(1)	254.4(11)	276.8(7)	1.2142(3)
AutoCorr (A-10)	5.0(5)	203.0(12)	721.2(8)	0.019290(13)	104.0(6)	546.8(12)	1.4653(9)
StanDeviCorr (A-11)	29.8(8)	4.8(1)	668.8(3)	0.000126(3)	252.6(9)	280.6(9)	1.1679(2)
Range (A-12)	35.6(13)	161.8(8)	789.2(11)	0.235540(16)	182.4(7)	227.2(5)	1.6766(14)
EntrAlgo (A-13)	28.2(7)	73.6(5)	675(5)	0.000731(8)	369.6(14)	153.4(2)	1.3332(5)
ThreCont (A-14)	33.2(12)	150.4(7)	793.8(16)	0.000552(4)	379.0(15)	216.6(4)	1.5582(11)
ThrePixeCont (A-15)	23.2(6)	44.0(4)	792(12)	0.009200(10)	84.0(5)	678.8(16)	1.4567(8)
ImagePower (A-16)	31.8(11)	169.8(9)	793.2(13)	0.001100(7)	401.8(16)	256.0(6)	1.6304(12)

and the lowest noise level. The contributions of these three individual criterion measures are clearly reflected in the best overall performance. Although the derivative-based algorithms have better accuracy, their noise sensitivity prevents them from providing better overall performance.

Together with our previous findings [5], we hypothesize that the Variance or the Normalized Variance algorithm provides the best overall performance for all non-fluorescence microscopy applications.

VI. CONCLUSION

This paper presented a comparison study in order to determine the optical focus algorithm for bright-field imaging of blood smear and pap smear samples. 8000 images were processed by applying 16 selected focus algorithms. A ranking methodology comprised of six individual criteria and one overall score was used for ranking the focus algorithms. The Variance algorithm was found to provide the best overall performance for both blood smear and pap smear samples. Thus, the Variance algorithm will be selected for our future implementation of automated microscopic systems for computer-assisted blood and pap evaluation.

REFERENCES

[1] J. Angulo and G. Flandrin, "Automated detection of working area of peripheral blood smears using mathematical morphology," *Ana. Cell Pathl.*, Vol. 25, No. 1, pp. 37-49, 2003.

[2] H. Simon, K. Voss, K. Wenzelides, P. Hufnagl, and K. Roth, "Automated microscopic image evaluation for histological diagnosis of tumours," *Exp. Pathol.*,Vol. 30, No. 1, pp. 51-58, 1986.

[3] D. Vollath, "Automatic focusing by correlative methods," *J. of Microscopy*, Vol.147, No. 3, pp. 279-288, 1987.

[4] D. Vollath, "The influence of the scene parameters and of noise on the behavior of automatic focusing algorithms," *J. of Microscopy*, Vol.151, No. 8, pp. 133-146, 1988.

[5] Y. Sun, S. Duthaler, B.J. Nelson, "Autofocusing in computer microscopy: selecting the optimal focus algorithm," *Microscopy Research and Technique*, Vol. 65, pp. 139-149, 2004.

[6] A. Santos, C.O. Solórzano, J.J. Vaquero, J.M. Peña, N. Malpica, and F. Pozo, "Evaluation of autofocus functions in molecular cytogenetic analysis," *J. of Microscopy*, Vol. 188, pp. 264-272, 1997.

[7] J. Brenner, B. Dew, J. Horton, J. King, P. Neirath, and W. Sellers, "An automated microscope for cytologic research," J. of Histochem. And Cytochem., Vol. 24, No. 1, pp. 100-111, 1971.

[8] T. Yeo, S.O. Jayasooriah, and R. Sinniah, "Autofocusing for tissue microscopy," *Image and Vis. Comput.*, Vol. 11, pp. 629-639, 1993.

[9] E. Krotov, "Focusing," *International J. of Computer Vision*, Vol. 1, pp. 223-237, 1987.

[10] M. Subbarao, T. Choi, and A. Nikzad, "Focusing techniques," *Optical Engineering*, Vol. 32, No. 11, pp. 2824-2836, 1993.

[11] S. Nayar and Y. Nakagawa, "Shape from focus," *IEEE Trans. Patern Anal. and Machine Intell.*, Vol. 16, No. 8, pp. 824-831, 1994.

[12] J.M. Geusebroek, F. Cornelissen, A. Smeulders, and H. Geerts, "Robust autofocusing in microscopy," *Cytom.*, Vol. 39, pp. 1-9, 2000.

[13] F. Groen, I.T. Young, and G. Ligntart, "A comparison of different focus functions for use in autofocus algorithms," *Cytometry*, Vol. 12, pp. 81-91, 1985

[14] L. Firestone, K. Gook, K. Gulp, N. Talsania, and K. Preston, "Comparison of autofocus methods for use in automated algorithms," *Cytometry*, Vol. 12, pp. 81-91, 1991.

[15] M.L. Mehdelsohn and B.H. Mayall, "Computer-oriented analysis of human chromosomes-III focus," *Comput. Biol. Med.*, Vol. 2, pp. 137-150, 1972.